ZTRS: ZERO-IMITATION END-TO-END AUTONOMOUS DRIVING WITH TRAJECTORY SCORING

Anonymous authors
Paper under double-blind review

ABSTRACT

End-to-end autonomous driving maps raw sensor inputs directly into ego-vehicle trajectories to avoid cascading errors from perception modules and to leverage rich semantic cues. Existing frameworks largely rely on Imitation Learning (IL), which can be limited by sub-optimal expert demonstrations and covariate shift during deployment. On the other hand, Reinforcement Learning (RL) has recently shown potential in scaling up with simulations, but is typically confined to low-dimensional symbolic inputs (e.g. 3D objects and maps), falling short of full end-to-end learning from raw sensor data. We introduce ZTRS (Zero-Imitation End-to-End Autonomous Driving with Trajectory Scoring), a framework that combines the strengths of both worlds: sensor inputs without losing information and RL training for robust planning. To the best of our knowledge, ZTRS is the first framework that eliminates IL entirely by only learning from rewards while operating directly on high-dimensional sensor data. ZTRS utilizes offline reinforcement learning with our proposed Exhaustive Policy Optimization (EPO), a variant of policy gradient tailored for enumerable actions and rewards. ZTRS demonstrates strong performance across three benchmarks: Navtest (generic real-world open-loop planning), Navhard (open-loop planning in challenging real-world and synthetic scenarios), and HUGSIM (simulated closed-loop driving). Specifically, ZTRS achieves the state-of-the-art result on Navhard and outperforms IL-based baselines on HUGSIM.

1 INTRODUCTION

End-to-end autonomous driving, which aims to map high-dimensional sensor data into an ego-vehicle trajectory with a neural planner, has emerged as a critical research direction. Unlike modularized approaches, where a privileged planner relies on low-dimensional symbolic inputs (e.g. 3D objects and map information), end-to-end methods avoid cascading errors from perception modules (Hu et al., 2023) and leverage rich semantic cues that privileged planners cannot access (Mu et al., 2024).

Two main paradigms have emerged for training planners: Imitation Learning (IL) and Reinforcement Learning (RL). IL requires human demonstrations for training, while RL requires reliable simulation environments. In current research, RL-based methods can scale with massive simulation data (Cusumano-Towner et al., 2025; Jaeger et al., 2025) and simple rewards (Jaeger et al., 2025). They demonstrate more robustness compared with IL-based counterparts, which often face covariate shift during deployment and rely on human demonstrations that can be either noisy or sub-optimal.

However, RL-based methods are still restricted to symbolic inputs. Scaling RL online with sensor data remains impractical: real-world exploration is unsafe, and large-scale sensor simulation is both costly and difficult to make realistic. For instance, diffusion-based world models (Guo et al., 2025; Agarwal et al., 2025) demand thousands of GPU hours just to approximate the scale of public datasets (Dauner et al., 2024).

To achieve the best of both worlds: preserving rich sensor inputs and leveraging reinforcement learning for robust planning, we propose ZTRS: **Z**ero-Imitation End-to-end Autonomous Driving with **TR**ajectory **S**coring, the first framework that eliminates imitation learning entirely from the end-to-end training pipeline.

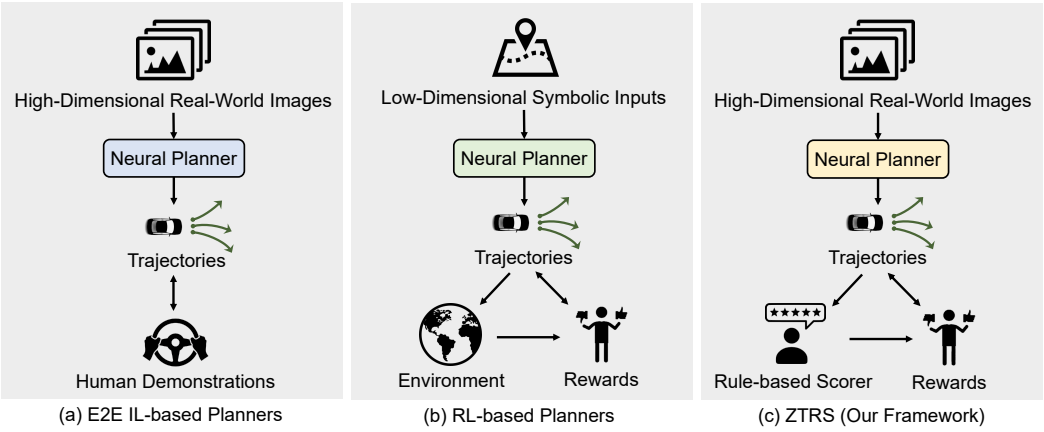

Figure 1: **Comparisons between three paradigms for end-to-end autonomous driving.**

ZTRS builds on three pillars: data, rewards, and policy optimization. For the data pillar, since large-scale sensor data collection is difficult, we rely on offline driving datasets. This naturally transforms our problem into offline reinforcement learning (Levine et al., 2020), where the planner learns to maximize the reward at each data point. For the reward pillar, this offline setting aligns with the open-loop trajectory planning problem (Dauner et al., 2023; Li et al., 2024c; Dauner et al., 2024) in the end-to-end autonomous driving literature, so we adopt the widely-used open-loop planning metrics (Dauner et al., 2024; Li et al., 2025b; Cao et al., 2025) as rewards, enabling efficient evaluation of safety, rule-compliance, and comfort.

The final pillar is policy optimization. Without human demonstrations, policy optimization suffers from the cold-start problem, as random exploration in the continuous trajectory space is highly inefficient (Lillicrap et al., 2015). To address this, we propose Exhaustive Policy Optimization (EPO), a variant of policy gradient designed for offline data and enumerable action spaces. By enumerating a rich trajectory set as the action space, EPO provides dense supervision by optimizing each action in the trajectory set rather than randomly sampled actions. This formulation allows us to efficiently train a high-capacity planner entirely in the offline setting, without imitation learning or additional environment interaction.

We evaluate ZTRS on three autonomous driving benchmarks: Navtest (Dauner et al., 2024) for generic real-world open-loop planning, Navhard (Cao et al., 2025) for planning in challenging real-world and synthetic scenarios, and HUGSIM (Zhou et al., 2024) for simulated closed-loop driving. Our experiments demonstrate that ZTRS exhibits general planning abilities comparable to IL-based planners while maintaining robustness in safety-critical driving situations. Notably, ZTRS establishes a new state-of-the-art on the open-loop planning benchmark Navhard and outperforms IL-based baselines on the closed-loop driving benchmark HUGSIM.

Our contributions are as follows:

1. We introduce ZTRS, a zero-imitation end-to-end autonomous driving framework with trajectory scoring. This framework is the first to solely learn from rewards rather than human demonstrations, while operating fully on high-dimensional real-world images.
2. We propose offline reinforcement learning with Exhaustive Policy Optimization, a variant of policy gradient tailored for enumerable actions and rewards. This optimization process allows us to efficiently train an end-to-end policy from scratch.
3. We evaluate ZTRS on three benchmarks: Navtest, Navhard, and HUGSIM. ZTRS demonstrates strong planning performance compared with other IL-based trajectory scorers under different evaluation protocols (i.e. open-loop planning and closed-loop driving) and diverse sensor data (i.e. real-world images and 3DGS-rendered images). It also achieves the state-of-the-art result on the challenging Navhard benchmark and outperforms IL-based baselines on HUGSIM.

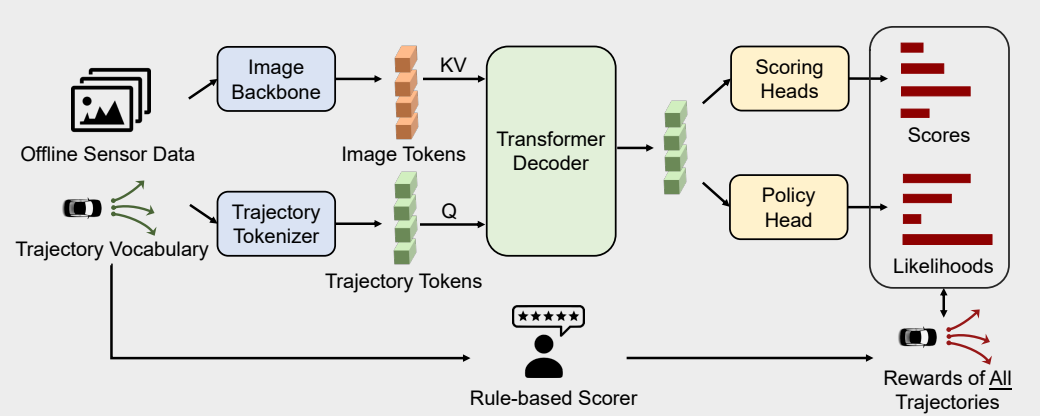

Figure 2: **The Overall Framework of ZTRS.** Given offline sensor data and a fixed set of trajectories, ZTRS first tokenizes these two modalities. In a Transformer Decoder, the trajectory tokens attend to image tokens to acquire the context. Finally, scoring heads and a policy head map the trajectory tokens to rule-based scores and action likelihoods.

2 METHODOLOGY

In this section, we elaborate on the framework and the policy optimization technique used in ZTRS.

2.1 OVERALL FRAMEWORK

As shown in Fig. 2, ZTRS is a trajectory scorer (Li et al., 2024b; 2025b;e; Wang et al., 2025; Sima et al., 2025; Yao et al., 2025; Li et al., 2025f), whose functionality is to score a discrete set of trajectories $\mathcal{A} = \{a_i\}_{i=1}^n$ instead of regressing to a continuous trajectory. The discrete formulation sidesteps the need for exploring in a large continuous space, also facilitating efficient reward computation in an offline manner.

ZTRS consists of five modules: an image backbone, a trajectory tokenizer, a Transformer Decoder, a policy head, and several scoring heads. The policy head produces probabilities for taking each action in $\mathcal{A}$, while the scoring heads predict the scores for each open-loop metric in the Extended Predictive Driver Model Score (EPDMS, $\mathcal{E}$) (Dauner et al., 2024; Li et al., 2025b; Cao et al., 2025). EPDMS evaluates multiple aspects of driving behavior (e.g., safety, progress, and rule compliance) and can be efficiently computed in an offline manner. Given a state s sampled from an offline dataset $\mathcal{D}$, where s contains sensor data and ego-vehicle status, the forward process involves three steps:

- The image backbone extracts L image tokens $\{x_{img}^i\}_{i=1}^L$ from a frontal-view image, while the trajectory tokenizer encodes trajectory candidates into queries $\{x_{traj}^i\}_{i=1}^n$.
- In the Transformer Decoder, the trajectory queries attend to image tokens.
- The policy head maps the attended trajectory queries $\{x_{traj}^i\}_{i=1}^n$ to probabilities $\pi(\cdot|s)$, and m scoring heads map them to m rule-based scores $\{\mathcal{S}_i(\cdot|s)\}_{i=1}^m$.

During training, the scoring heads are trained with binary classification losses against $\mathcal{E}(s, \cdot)$, while the policy head is trained with Exhaustive Policy Optimization (See Sec. 2.3). At inference, the final trajectory $a \in \mathcal{A}$ is chosen using a weighted average of $m + 1$ scores: $\pi(\cdot|s)$ and $\{\mathcal{S}_i(\cdot|s)\}_{i=1}^m$.

2.2 PRELIMINARY: THE POLICY GRADIENT THEOREM

To optimize a trajectory scorer with only rewards, we start with a simplified one-step policy optimization problem where the action space is a finite discrete set $\mathcal{A}$, and π is a policy parameterized by θ. In the online RL setting (Sutton et al., 1998), the action a is sampled with $\pi(a|s)$, where s is the current state. In our offline RL setting (Levine et al., 2020), the state s is sampled from an offline

dataset $\mathcal{D}$. Following the notation of Schulman et al. (2015), the policy gradient g is defined as

$$g := \mathbb{E}\left[\Psi(s,a)\nabla_\theta \log \pi_\theta(a \mid s)\right], \tag{1}$$

where the advantage function $\Psi(s,a)$ can represent many quantities, such as the cumulative return or the state-action value function. The gradient can be equivalently written as

$$\begin{aligned} g &= \mathbb{E}\left[\Psi(s,a)\nabla_\theta \log \pi_\theta(a \mid s)\right] && (2)\\ &= \sum_{a' \in \mathcal{A}} \Psi(s,a')\pi_\theta(a' \mid s)\, \nabla_\theta \log \pi_\theta(a' \mid s) && (3)\\ &= \sum_{a' \in \mathcal{A}} \Psi(s,a')\pi_\theta(a' \mid s)\, \frac{\nabla_\theta \pi_\theta(a' \mid s)}{\pi_\theta(a' \mid s)} && (4)\\ &= \sum_{a' \in \mathcal{A}} \Psi(s,a')\nabla_\theta \pi_\theta(a' \mid s). && (5) \end{aligned}$$

This formulation matches the classical Policy Gradient Theorem (Sutton et al., 1999). Notably, the summation over all actions in $\mathcal{A}$ suggests that if the advantage function Ψ can be computed for each action at state s, policy optimization can be carried out directly on action likelihoods rather than log-likelihoods, as shown in Eq. 5.

2.3 Offline Reinforcement Learning with Exhaustive Policy Optimization

When the action space $\mathcal{A}$ is a set of trajectories covering almost all driving possibilities, policy optimization can be formulated as maximizing the objective for an offline dataset $\mathcal{D}$

$$\mathbb{E}_{s\sim\mathcal{D},\, a\sim\mathcal{A}}\left[\Psi(s,a)\right]. \tag{6}$$

This is consistent with the one-step policy optimization problem in Sec. 2.2 if Ψ is derived from open-loop reward signals, which do not require additional environment interaction. This objective can be optimized either in the log-likelihood form on a sampled action (Eq. 1) or in the likelihood form on the entire action space (Eq. 5). The latter formulation,

$$g := \sum_{\substack{a' \in \mathcal{A} \\ s \sim \mathcal{D}}} \Psi(s,a')\, \nabla_\theta \pi_\theta(a' \mid s) \tag{7}$$

provides much denser supervision for the policy. Eq. 7 also defines our proposed *Exhaustive Policy Optimization (EPO)*, a variant of policy gradient tailored for offline data and enumerable actions. Specifically, EPO optimizes the policy by exhaustively considering every possible action $a \in \mathcal{A}$ and its respective advantage $\Psi(s,a)$. An overview of the pipeline is shown in Fig. 2.

To compute the advantage function Ψ, we adopt the EPDMS metric score $\mathcal{E}$ for its efficient and comprehensive evaluation of trajectories. Specifically, $\mathcal{E}$ can cover safety, rule-compliance, and progress for each state-action pair (s,a). The scores $\mathcal{E}(s,\cdot)$ can also be reused for each state $s \in \mathcal{D}$ since the action space is fixed throughout the training process. To further enforce temporal consistency, we subtract a correction term $b(s_t, a_t, a_{t-1}) = \lambda \mathbb{1}\left[\text{EC}(a_{t-1}, a_t)\right]$, where λ is a constant, $a_{t-1} = \underset{a}{\text{argmax}}\pi(a|s_{t-1})$, and EC indicates the violation of Extended Comfort (EC) thresholds (Li et al., 2025b):

$$\Psi(s_t, a_t) = \mathcal{E}(s_t, a_t) - b(s_t, a_t, a_{t-1}). \tag{8}$$

Note that this formulation penalizes inconsistent predictions more strongly than the one used in Li et al. (2025b); Cao et al. (2025). Finally, Ψ is normalized to zero mean and unit variance following Huang et al. (2022); Shao et al. (2024).

3 Experiments

3.1 Dataset and Metrics

Dataset. We conduct experiments on three benchmarks, including Navtest (Dauner et al., 2024), Navhard (Cao et al., 2025), and HUGSIM (Zhou et al., 2024).

Navtest (Dauner et al., 2024) is the evaluation dataset used in NAVSIM. NAVSIM contains 103k and 12k diverse and challenging driving scenarios for model training (Navtrain) and evaluation (Navtest), and introduces simulation-based metrics to better review closed-loop planning capability through open-loop evaluation. During evaluation, the output trajectory is evaluated by a simulator to get rule-based simulation metric scores related to multiple driving aspects, such as traffic rule compliance, comfort, and progress.

Navhard (Cao et al., 2025) further proposes pseudo-simulation on the challenging scenarios in NAVSIM, extending the evaluation to a two-stage paradigm. The first stage follows the original NAVSIM evaluation, while the second stage adopts 3D Gaussian Splatting (3DGS) (Kerbl et al., 2023; Li et al., 2025c) to synthesize subsequent driving scenarios, resulting in 244 initial scenarios and 4164 synthetic scenarios.

HUGSIM (Zhou et al., 2024) is a closed-loop driving benchmark featuring 3DGS-synthesized images. It integrates multiple driving datasets, including KITTI-360 (Liao et al., 2022), Waymo (Sun et al., 2020), nuScenes (Caesar et al., 2020), and Pandaset (Xiao et al., 2021), into a collection of 345 driving scenarios. These scenarios are categorized by difficulty into four levels: easy, medium, hard, and extreme. Specifically, HUGSIM released 49 easy scenarios for regular driving, 126 medium scenarios with inserted vehicles, and 86 hard scenarios as well as 84 extreme scenarios with aggressive vehicles.

Metrics. Navtest and Navhard evaluate open-loop planning with EPDMS $\mathcal{E}(s, a)$:

$$\mathcal{E}(s,a) = \left(\prod_{m \in S_{\text{pen}}} m(s,a) \right) \cdot \left(\frac{\sum_{m \in S_{\text{avg}}} w_m \, m(s,a)}{\sum_{m \in S_{\text{avg}}} w_m} \right), \tag{9}$$

where s is the current state and a is a 4-second trajectory. The penalty metric set S_{pen} is applied multiplicatively and includes No-at-fault Collisions (NC), Drivable Area Compliance (DAC), Driving Direction Compliance (DDC), and Traffic Light Compliance (TLC), while the weighted metric set S_{avg} contains Time-to-Collision (TTC), Ego Progress (EP), Lane Keeping (LK), and History Comfort (HC). The extended comfort (EC) from Li et al. (2025b) is also used as a weighted metric to promote temporally consistent driving. w_m is the aggregation weight for metric m. Note that human filtering is used in Cao et al. (2025) for calculating $\mathcal{E}$ but not in our training. For HUGSIM, HD-Score is used for closed-loop evaluation. It aggregates Route Completion (RC) with NC, DAC, TTC, HC across an episode of length T:

$$\text{HD-Score} = RC \cdot \sum_{t=1}^{T} \left(\prod_{m \in \{NC, DAC\}} m(s_t, \tilde{a}_t) \right) \cdot \left(\frac{\sum_{m \in \{TTC, HC\}} w_m \, m(s_t, \tilde{a}_t)}{\sum_{m \in \{TTC, HC\}} w_m} \right), \tag{10}$$

where $\tilde{a}$ is the ego-vehicle acceleration and steering angle transformed from a trajectory.

3.2 Implementation Details

All our models are trained on the Navtrain split with 24 NVIDIA A100 GPUs, while the synthetic data from Navhard and HUGSIM are not used for training. Models are trained for 15 epochs with a total batch size of 528, using a learning rate and weight decay of 2×10^{-4} and 0.0. The frontal view with center-cropped front-left and front-right views are concatenated as the input image, which is then resized to 512×2048. The hyperparameter λ in the correction term b is set to 0.2. By default, the action space used in our method has 16384 trajectories, each spanning 4 seconds at 10Hz. These trajectories are obtained through K-means clustering on the nuPlan dataset (H. Caesar, 2021). Following Li et al. (2024b; 2025b); Yao et al. (2025), we default to use the DD3D-pretrained (Park et al., 2021) V2-99 (Lee et al., 2019) as the image backbone in our experiments. The ViT-L Dosovitskiy et al. (2020) backbone is pretrained from Depth-Anything (Yang et al., 2024).

3.3 Quantitative Results

Table 1 reports performance on the challenging Navhard benchmark. Compared with IL-based methods, ZTRS achieves superior scores across most safety and comfort metrics, attaining the highest overall EPDMS (45.5%) with the V2-99 backbone. Further, Tab. 2 shows performance on

Table 1: **Performance on the Navhard Benchmark.** PDM-Closed uses ground-truth symbolic inputs for planning, while other methods rely on sensor data.

Method	IL	Backbone	Stage	NC	DAC	DDC	TLC	EP	TTC	LK	HC	EC	EPDMS
PDM-Closed (Dauner et al., 2023)	✗	-	Stage 1	94.4	98.8	100	99.5	100	93.5	99.3	87.7	36.0	51.3
			Stage 2	88.1	90.6	96.3	98.5	100	83.1	73.7	91.5	25.4	
LTF (Chitta et al., 2022)	✓	ResNet34	Stage 1	96.2	79.5	99.1	99.5	84.1	95.1	94.2	97.5	79.1	23.1
			Stage 2	77.7	70.2	84.2	98.0	85.1	75.6	45.4	95.7	75.9	
DriveSuprim (Yao et al., 2025)	✓	V2-99	Stage 1	98.9	95.1	99.2	99.6	76.1	99.1	94.7	97.6	54.2	42.1
			Stage 2	87.9	88.8	89.6	98.8	80.3	86.0	53.5	97.1	56.1	
		EVA-ViT-L	Stage 1	98.7	98.0	99.1	99.8	75.9	98.7	94.7	97.6	49.8	44.7
			Stage 2	89.5	89.6	92.9	98.5	78.9	86.4	55.3	96.5	52.7	
		ViT-L	Stage 1	97.8	97.3	98.9	99.3	77.1	98.2	95.8	97.6	50.2	43.4
			Stage 2	90.3	88.9	90.8	98.9	81.1	87.4	54.2	95.1	48.3	
GTRS-Dense (Li et al., 2025f)	✓	V2-99	Stage 1	98.7	95.8	99.4	99.3	72.8	98.7	95.1	96.9	40.4	41.7
			Stage 2	91.4	89.2	94.4	98.8	69.5	90.1	54.6	94.1	49.7	
		EVA-ViT-L	Stage 1	97.6	95.8	99.7	99.8	77.2	97.8	95.3	97.3	46.7	43.4
			Stage 2	91.9	91.3	92.7	99.0	72.7	90.4	53.8	94.1	41.6	
		ViT-L	Stage 1	98.9	98.2	99.8	99.6	73.9	98.9	95.3	97.3	40.0	45.3
			Stage 2	91.5	90.8	94.7	98.5	70.8	90.1	55.4	97.2	54.2	
ZTRS (Ours)	✗	ViT-L	Stage 1	98.6	96.7	99.8	99.8	72.1	98.0	95.6	97.6	51.6	45.0
			Stage 2	88.9	90.9	94.6	97.9	70.8	87.1	58.6	97.5	63.6	
		V2-99	Stage 1	98.9	97.6	100.0	100.0	66.7	98.9	96.2	96.7	44.0	**45.5**
			Stage 2	91.1	90.4	95.8	99.0	63.6	89.8	60.4	97.6	66.1	

Table 2: **Performance on the Navtest Benchmark.**

Method	IL	Backbone	NC ↑	DAC ↑	DDC ↑	TL ↑	EP ↑	TTC ↑	LK ↑	HC ↑	EC ↑	EPDMS ↑
Human Agent	-	-	100	100	99.8	100	87.4	100	100	98.1	90.1	90.3
Ego Status MLP	✓	-	93.1	77.9	92.7	99.6	86.0	91.5	89.4	98.3	85.4	64.0
Transfuser (Chitta et al., 2022)	✓	ResNet34	96.9	89.9	97.8	99.7	87.1	95.4	92.7	98.3	87.2	76.7
HydraMDP++ (Li et al., 2025b)	✓	ResNet34	97.2	97.5	99.4	99.6	83.1	96.5	94.4	98.2	70.9	81.4
		V2-99	98.4	98.0	99.4	99.8	87.5	97.7	95.3	98.3	77.4	85.1
		ViT-L	98.5	98.5	99.5	99.7	87.4	97.9	95.8	98.2	75.7	85.6
DriveSuprim (Yao et al., 2025)	✓	ResNet34	97.5	96.5	99.4	99.6	88.4	96.6	95.5	98.3	77.0	83.1
		V2-99	97.8	97.9	99.5	99.9	90.6	97.1	96.6	98.3	77.9	86.0
		ViT-L	98.4	98.6	99.6	99.8	90.5	97.8	97.0	98.3	78.6	**87.1**
ZTRS (Ours)	✗	V2-99	97.8	99.4	99.8	99.8	84.1	97.0	96.2	98.2	77.2	85.3
		ViT-L	98.2	99.1	99.7	99.8	86.9	97.5	96.6	98.2	78.2	86.2

Table 3: **Zero-shot Performance on the HUGSIM Benchmark.** *Official results from Zhou et al. (2024) on both public and unreleased private scenarios. The rest are based on the public scenarios.

Method	Easy		Medium		Hard		Extreme		Overall	
	RC	HD-Score	RC	HD-Score	RC	HD-Score	RC	HD-Score	RC	HD-Score
UniAD (Hu et al., 2023)*	58.6	48.7	41.2	29.5	40.4	27.3	26.0	14.3	40.6	28.9
VAD (Jiang et al., 2023)*	38.7	24.3	27.0	9.9	25.5	10.4	23.0	8.2	27.9	12.3
LTF (Chitta et al., 2022)*	68.4	52.8	40.7	24.6	36.9	19.8	25.5	8.1	41.4	24.8
LTF (Chitta et al., 2022)	60.4	42.5	39.4	17.7	32.7	11.8	27.9	10.6	37.9	18.0
GTRS-Dense (Li et al., 2025f)	64.2	55.5	50.0	39.0	20.7	11.7	22.3	14.3	38.0	28.6
ZTRS (Ours)	74.4	60.8	50.9	34.2	32.7	20.5	21.9	11.0	**42.6**	**28.9**

the real-world Navtest benchmark. ZTRS achieves better open-loop planning performance than Hydra-MDP++ (Li et al., 2025b) with both V2-99 and ViT-L backbones, but still falls behind DriveSuprim (Yao et al., 2025), which utilizes more advanced data augmentation techniques and scoring architectures. Finally, Tab. 3 shows the zero-shot performance on the HUGSIM benchmark. Without adaptation to simulated data or closed-loop driving, ZTRS achieves the best RC and HD-Score on public scenarios, outperforming IL-based GTRS-Dense by 4.6% RC and 0.3% HD-Score.

3.4 Ablation Study

In Tab. 4, we study the effects of different learning paradigms and targets. When using the trajectory with the maximum EPDMS score (i.e., $\hat{\mathcal{E}} = \underset{a}{\text{argmax}}\mathcal{E}(s, a)$) as the imitation target, perfor-

Table 4: **Ablation study on different learning paradigms and targets.** $\hat{\mathcal{E}}$ represents using the trajectory with the maximum ground-truth EPDMS as the imitation target, while ll and log-ll represent optimization with likelihoods over all actions and the log-likelihood over a sampled action.

IL	RL	Target	NC ↑	DAC ↑	DDC ↑	TL ↑	EP ↑	TTC ↑	LK ↑	HC ↑	EC ↑	EPDMS ↑
✓	✗	Human	98.5	98.7	98.9	99.9	88.5	98.2	97.0	98.3	80.5	86.2
✓	✗	$\hat{\mathcal{E}}$	96.6	96.8	99.5	99.6	88.3	96.0	96.7	92.2	18.5	76.7
✗	ll	$\mathcal{E}$	97.5	99.2	99.8	99.7	89.3	96.9	96.8	98.0	53.8	84.2
✗	ll	$\mathcal{E} - b$	97.8	99.4	99.8	99.8	84.1	97.0	96.2	98.2	77.2	**85.3**
✗	log-ll	$\mathcal{E} - b$	97.7	96.7	99.7	99.9	73.0	96.1	93.2	97.7	36.1	75.0

Table 5: **The relationship between the size of the action space and evaluation data.** EPDMS_1 measures the real-world portion of Navhard, while EPDMS_2 measures the simulated portion.

Backbone	$\lvert\mathcal{A}\rvert$ for training	$\lvert\mathcal{A}\rvert$ for inference	Navtest	Navhard		
			EPDMS	EPDMS_1	EPDMS_2	EPDMS
V2-99	8192	8192	84.6	73.3	57.4	43.0
	16384	16384	**85.3**	**74.9**	57.1	43.4
	16384	8192	82.0	74.2	**60.7**	**45.5**
ViT-L	8192	8192	84.6	73.7	55.9	41.9
	16384	16384	**86.2**	**76.1**	50.5	38.8
	16384	8192	84.3	73.4	**59.9**	**45.0**

mance drops significantly compared to the IL baseline, as many trajectories in $\mathcal{A}$ can achieve high EPDMS and a single target fails to capture the underlying pattern. Using likelihoods over the entire action space mitigates this issue, improving EPDMS by 7.5%, but introduces serious oscillation, as indicated by the low EC metric. This highlights the need for our correction term b to enforce temporal consistency. Using $\mathcal{E} - b$ as the reward increases EC by 23.4%. In contrast, computing log-likelihoods over a sampled action fails to perform equally, which demonstrates the effectiveness of our EPO method in providing dense supervision for the entire action space.

Tab. 5 shows the relationship between the size of the action space and evaluation data. We observe that models using the full action space during inference achieve the best results on real-world data, as reflected by EPDMS on Navtest and Navhard, while shrinking the action space improves performance on the simulated portion. This finding is consistent with GTRS (Li et al., 2025f): regardless of whether the model is trained with human demonstrations, reducing model complexity tends to enhance generalization on unseen simulated data.

3.5 Qualitative Results.

Fig. 3 and Fig. 4 show visualization results on the open-loop planning benchmark Navtest and the closed-loop driving benchmark HUGSIM, respectively. Interestingly, ZTRS learns driving patterns that resemble human trajectories from rule-based rewards, though it is trained without human demonstrations. Moreover, ZTRS manages to navigate safely in safety-critical driving scenarios without training on simulated data, as shown in Fig. 4. Even under the extreme condition depicted in Fig. 4 (c), where the ego agent must overtake a parked car while facing an oncoming vehicle, ZTRS can safely complete the route. This demonstrates the strong closed-loop driving ability of ZTRS.

4 Related Work

4.1 End-to-end Imitation Learning for Autonomous Driving

Given an offline expert dataset, Imitation Learning (IL) trains a policy to mimic expert behavior. In the end-to-end autonomous driving literature (Chen et al., 2024a), early IL-based approaches (Codevilla et al., 2018) proved effective in the closed-loop driving simulator

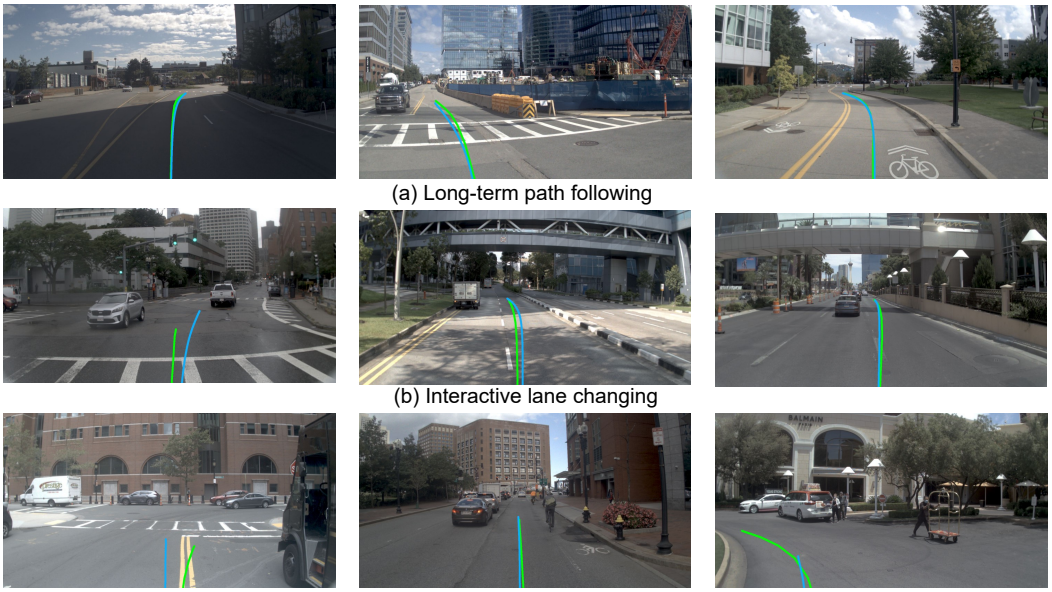

(a) Long-term path following

(b) Interactive lane changing

(c) Cautious driving near parked vehicles and pedestrians

Figure 3: **Visualizations of planned trajectories (blue curves) and the human trajectory (green curves) on the open-loop planning benchmark Navtest.**

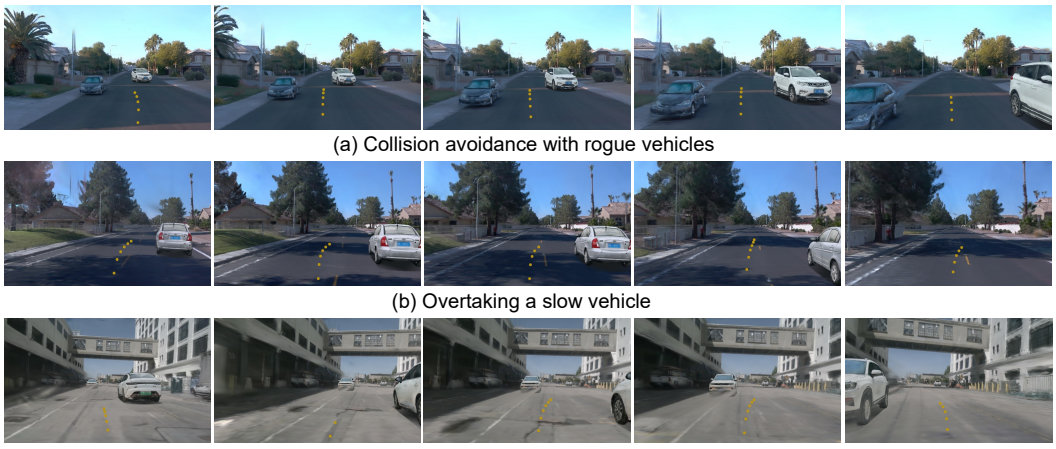

(a) Collision avoidance with rogue vehicles

(b) Overtaking a slow vehicle

(c) Overtaking with oncoming traffic

Figure 4: **Visualizations of planned trajectories (orange dots) on the challenging closed-loop driving benchmark HUGSIM.**

CARLA (Dosovitskiy et al., 2017). Subsequent works improve the closed-loop driving performance with modern neural architectures (e.g. Transformers (Vaswani et al., 2017)) (Chitta et al., 2022), intermediate representations (Hu et al., 2022; Renz et al., 2022; Shao et al., 2023; Jia et al., 2023b), and policy distillation (Chen et al., 2020; Zhang et al., 2021; Wu et al., 2022; Jia et al., 2023a). The introduction of UniAD (Hu et al., 2023) highlighted the strength of IL on real-world sensor data, whose complexity and diversity greatly exceed synthetic data produced by simulators. Building on this foundation, numerous efforts further focus on efficiency (Jiang et al., 2023; Liao et al., 2025), multi-modal behaviors (Chen et al., 2024b; Liao et al., 2025), vision-language understanding (Wang et al., 2024; Li et al., 2025d), and safety constraints (Li et al., 2024b).

4.2 Reinforcement Learning for Autonomous Driving

Unlike Imitation Learning, Reinforcement Learning (RL) (Sutton et al., 1998) trains agents to maximize rewards by interacting with the environment, and autonomous driving RL methods generally fall into two categories: symbolic-input methods and sensor-based methods, both relying on simulators. Symbolic-input methods (Toromanoff et al., 2020; Zhang et al., 2021; Li et al., 2024a; Cusumano-Towner et al., 2025; Jaeger et al., 2025) use low-dimensional abstractions (e.g. 3D bounding boxes, maps, traffic signals) and have shown strong results on CARLA (Dosovitskiy et al., 2017), nuPlan (H. Caesar, 2021), and Waymax (Gulino et al., 2023). GigaFlow (Cusumano-Towner et al., 2025) and CaRL (Jaeger et al., 2025) both demonstrated that large-scale RL could train robust policies from scratch. On the other hand, sensor-based approaches operate on raw inputs like images. Early attempts (Kendall et al., 2019) explored real-world training, but faced safety and efficiency challenges, while subsequent works (Nehme & Deo, 2023; Delavari et al., 2025; Yang et al., 2025) relied on simulated sensor data in CARLA. Despite success in simulators, such approaches could face sim-to-real gaps. Recently, RAD (Gao et al., 2025) fine-tuned a policy in a 3DGS simulator with high-dimensional real-world images, but still depended on human demonstrations for pre-training and reward computation. Similarly, several other approaches avoid the cold-start problem by fine-tuning an IL-pretrained diffusion policy (Li et al., 2025d;a). In contrast, our approach learns trajectory planning with reward signals from scratch, while operating on high-dimensional real-world sensor data.

4.3 Scoring-based End-to-end Trajectory Planning

The scoring-based end-to-end planning method introduces a predefined vocabulary containing multiple trajectories, and scores each trajectory to select the most appropriate candidate as the output. Early works (Philion & Fidler, 2020; Phan-Minh et al., 2020; Chen et al., 2024b) score the trajectory candidates through classification based on their distance towards the ground-truth human trajectory. Beyond relying on a single human demonstration, the Hydra-MDP series (Li et al., 2024b; 2025b) proposed multi-target hydra-distillation to score trajectories with multiple rule-based metrics, leading to more robust planning capability. SafeFusion (Wang et al., 2025) synthesizes collision-related scenarios for training a robust planning model and eases the reliance on imitation learning. Other works further introduce multiple approaches to reach more precise and comprehensive trajectory scoring, such as test-time training (Sima et al., 2025), iterative refinement (Yao et al., 2025), and diffusion-based trajectory generation (Li et al., 2025e;f). Despite these advancements, these scorers still rely heavily on the imitation of human trajectories. In contrast, our approach fully discards expert demonstrations and achieves strong end-to-end planning performance via reinforcement learning.

5 Conclusion

We present ZTRS, the first end-to-end autonomous driving framework that eliminates imitation learning. In summary, ZTRS demonstrates that end-to-end planners can be trained entirely without human demonstrations by leveraging offline data, reward-driven supervision, and Exhaustive Policy Optimization. By densely optimizing over enumerable actions, ZTRS overcomes the cold-start problem and achieves robust planning by operating on high-dimensional sensor inputs. Extensive evaluations on real-world and simulated benchmarks show that ZTRS not only matches or exceeds IL-based planners in planning capabilities but also establishes new state-of-the-art performance in challenging and safety-critical conditions. These results highlight the potential of relying on rewards rather than human demonstrations to achieve reliable end-to-end autonomous driving.

References

Niket Agarwal, Arslan Ali, Maciej Bala, Yogesh Balaji, Erik Barker, Tiffany Cai, Prithvijit Chattopadhyay, Yongxin Chen, Yin Cui, Yifan Ding, et al. Cosmos world foundation model platform for physical ai. *arXiv preprint arXiv:2501.03575*, 2025.

Holger Caesar, Varun Bankiti, Alex H Lang, Sourabh Vora, Venice Erin Liong, Qiang Xu, Anush Krishnan, Yu Pan, Giancarlo Baldan, and Oscar Beijbom. nuscenes: A multimodal dataset for autonomous driving. In *CVPR*, pp. 11621–11631, 2020.

Wei Cao, Marcel Hallgarten, Tianyu Li, Daniel Dauner, Xunjiang Gu, Caojun Wang, Yakov Miron, Marco Aiello, Hongyang Li, Igor Gilitschenski, et al. Pseudo-simulation for autonomous driving. *CoRL*, 2025.

Dian Chen, Brady Zhou, Vladlen Koltun, and Philipp Krähenbühl. Learning by cheating. In *CoRL*, pp. 66–75. PMLR, 2020.

Li Chen, Penghao Wu, Kashyap Chitta, Bernhard Jaeger, Andreas Geiger, and Hongyang Li. End-to-end autonomous driving: Challenges and frontiers. *IEEE Transactions on Pattern Analysis and Machine Intelligence*, 2024a.

Shaoyu Chen, Bo Jiang, Hao Gao, Bencheng Liao, Qing Xu, Qian Zhang, Chang Huang, Wenyu Liu, and Xinggang Wang. Vadv2: End-to-end vectorized autonomous driving via probabilistic planning. *arXiv preprint arXiv:2402.13243*, 2024b.

Kashyap Chitta, Aditya Prakash, Bernhard Jaeger, Zehao Yu, Katrin Renz, and Andreas Geiger. Transfuser: Imitation with transformer-based sensor fusion for autonomous driving. *IEEE Transactions on Pattern Analysis and Machine Intelligence*, 2022.

Felipe Codevilla, Matthias Müller, Antonio López, Vladlen Koltun, and Alexey Dosovitskiy. End-to-end driving via conditional imitation learning. In *ICRA*, pp. 4693–4700. IEEE, 2018.

Marco Cusumano-Towner, David Hafner, Alex Hertzberg, Brody Huval, Aleksei Petrenko, Eugene Vinitsky, Erik Wijmans, Taylor Killian, Stuart Bowers, Ozan Sener, et al. Robust autonomy emerges from self-play. *arXiv preprint arXiv:2502.03349*, 2025.

Daniel Dauner, Marcel Hallgarten, Andreas Geiger, and Kashyap Chitta. Parting with misconceptions about learning-based vehicle motion planning. In *Conference on Robot Learning*, pp. 1268–1281. PMLR, 2023.

Daniel Dauner, Marcel Hallgarten, Tianyu Li, Xinshuo Weng, Zhiyu Huang, Zetong Yang, Hongyang Li, Igor Gilitschenski, Boris Ivanovic, Marco Pavone, Andreas Geiger, and Kashyap Chitta. Navsim: Data-driven non-reactive autonomous vehicle simulation and benchmarking. In *NeurIPS*, 2024.

Elahe Delavari, Feeza Khan Khanzada, and Jaerock Kwon. A comprehensive review of reinforcement learning for autonomous driving in the carla simulator. *arXiv preprint arXiv:2509.08221*, 2025.

Alexey Dosovitskiy, German Ros, Felipe Codevilla, Antonio Lopez, and Vladlen Koltun. Carla: An open urban driving simulator. In *Conference on robot learning*, pp. 1–16. PMLR, 2017.

Alexey Dosovitskiy, Lucas Beyer, Alexander Kolesnikov, Dirk Weissenborn, Xiaohua Zhai, Thomas Unterthiner, Mostafa Dehghani, Matthias Minderer, Georg Heigold, Sylvain Gelly, et al. An image is worth 16x16 words: Transformers for image recognition at scale. *arXiv preprint arXiv:2010.11929*, 2020.

Hao Gao, Shaoyu Chen, Bo Jiang, Bencheng Liao, Yiang Shi, Xiaoyang Guo, Yuechuan Pu, Haoran Yin, Xiangyu Li, Xinbang Zhang, et al. Rad: Training an end-to-end driving policy via large-scale 3dgs-based reinforcement learning. *arXiv preprint arXiv:2502.13144*, 2025.

Cole Gulino, Justin Fu, Wenjie Luo, George Tucker, Eli Bronstein, Yiren Lu, Jean Harb, Xinlei Pan, Yan Wang, Xiangyu Chen, et al. Waymax: An accelerated, data-driven simulator for large-scale autonomous driving research. *NeurIPS*, 36:7730–7742, 2023.

Jiazhe Guo, Yikang Ding, Xiwu Chen, Shuo Chen, Bohan Li, Yingshuang Zou, Xiaoyang Lyu, Feiyang Tan, Xiaojuan Qi, Zhiheng Li, and Hao Zhao. Dist-4d: Disentangled spatiotemporal diffusion with metric depth for 4d driving scene generation. *arXiv preprint arXiv:2503.15208*, 2025.

K. Tan et al. H. Caesar, J. Kabzan. Nuplan: A closed-loop ml-based planning benchmark for autonomous vehicles. In *CVPR ADP3 workshop*, 2021.

Anthony Hu, Gianluca Corrado, Nicolas Griffiths, Zachary Murez, Corina Gurau, Hudson Yeo, Alex Kendall, Roberto Cipolla, and Jamie Shotton. Model-based imitation learning for urban driving. *NeurIPS*, 35:20703–20716, 2022.

Yihan Hu, Jiazhi Yang, Li Chen, Keyu Li, Chonghao Sima, Xizhou Zhu, Siqi Chai, Senyao Du, Tianwei Lin, Wenhai Wang, et al. Planning-oriented autonomous driving. In *CVPR*, pp. 17853–17862, 2023.

Shengyi Huang, Rousslan Fernand Julien Dossa, Chang Ye, Jeff Braga, Dipam Chakraborty, Kinal Mehta, and JoÃĢo GM AraÃšjo. Cleanrl: High-quality single-file implementations of deep reinforcement learning algorithms. *Journal of Machine Learning Research*, 23(274):1–18, 2022.

Bernhard Jaeger, Daniel Dauner, Jens Beißwenger, Simon Gerstenecker, Kashyap Chitta, and Andreas Geiger. Carl: Learning scalable planning policies with simple rewards. *arXiv preprint arXiv:2504.17838*, 2025.

Xiaosong Jia, Yulu Gao, Li Chen, Junchi Yan, Patrick Langechuan Liu, and Hongyang Li. Driveadapter: Breaking the coupling barrier of perception and planning in end-to-end autonomous driving. In *ICCV*, pp. 7953–7963, 2023a.

Xiaosong Jia, Penghao Wu, Li Chen, Jiangwei Xie, Conghui He, Junchi Yan, and Hongyang Li. Think twice before driving: Towards scalable decoders for end-to-end autonomous driving. In *CVPR*, pp. 21983–21994, 2023b.

Bo Jiang, Shaoyu Chen, Qing Xu, Bencheng Liao, Jiajie Chen, Helong Zhou, Qian Zhang, Wenyu Liu, Chang Huang, and Xinggang Wang. Vad: Vectorized scene representation for efficient autonomous driving. In *Proceedings of the IEEE/CVF International Conference on Computer Vision*, pp. 8340–8350, 2023.

Alex Kendall, Jeffrey Hawke, David Janz, Przemyslaw Mazur, Daniele Reda, John-Mark Allen, Vinh-Dieu Lam, Alex Bewley, and Amar Shah. Learning to drive in a day. In *ICRA*, pp. 8248–8254. IEEE, 2019.

Bernhard Kerbl, Georgios Kopanas, Thomas Leimkühler, and George Drettakis. 3d gaussian splatting for real-time radiance field rendering. *ACM Trans. Graph.*, 42(4):139–1, 2023.

Youngwan Lee, Joong-won Hwang, Sangrok Lee, Yuseok Bae, and Jongyoul Park. An energy and gpu-computation efficient backbone network for real-time object detection. In *Proceedings of the IEEE/CVF conference on computer vision and pattern recognition workshops*, pp. 0–0, 2019.

Sergey Levine, Aviral Kumar, George Tucker, and Justin Fu. Offline reinforcement learning: Tutorial, review, and perspectives on open problems. *arXiv preprint arXiv:2005.01643*, 2020.

Derun Li, Jianwei Ren, Yue Wang, Xin Wen, Pengxiang Li, Leimeng Xu, Kun Zhan, Zhongpu Xia, Peng Jia, Xianpeng Lang, et al. Finetuning generative trajectory model with reinforcement learning from human feedback. *arXiv preprint arXiv:2503.10434*, 2025a.

Kailin Li, Zhenxin Li, Shiyi Lan, Yuan Xie, Zhizhong Zhang, Jiayi Liu, Zuxuan Wu, Zhiding Yu, and Jose M Alvarez. Hydra-mdp++: Advancing end-to-end driving via expert-guided hydra-distillation. *arXiv preprint arXiv:2503.12820*, 2025b.

Qifeng Li, Xiaosong Jia, Shaobo Wang, and Junchi Yan. Think2drive: Efficient reinforcement learning by thinking with latent world model for autonomous driving (in carla-v2). In *ECCV*, pp. 142–158. Springer, 2024a.

Tianyu Li, Yihang Qiu, Zhenhua Wu, Carl Lindström, Peng Su, Matthias Nießner, and Hongyang Li. Mtgs: Multi-traversal gaussian splatting. *arXiv preprint arXiv:2503.12552*, 2025c.

Yongkang Li, Kaixin Xiong, Xiangyu Guo, Fang Li, Sixu Yan, Gangwei Xu, Lijun Zhou, Long Chen, Haiyang Sun, Bing Wang, et al. Recogdrive: A reinforced cognitive framework for end-to-end autonomous driving. *arXiv preprint arXiv:2506.08052*, 2025d.

Zhenxin Li, Kailin Li, Shihao Wang, Shiyi Lan, Zhiding Yu, Yishen Ji, Zhiqi Li, Ziyue Zhu, Jan Kautz, Zuxuan Wu, et al. Hydra-mdp: End-to-end multimodal planning with multi-target hydra-distillation. *arXiv preprint arXiv:2406.06978*, 2024b.

Zhenxin Li, Shihao Wang, Shiyi Lan, Zhiding Yu, Zuxuan Wu, and Jose M Alvarez. Hydra-next: Robust closed-loop driving with open-loop training. *ICCV*, 2025e.

Zhenxin Li, Wenhao Yao, Zi Wang, Xinglong Sun, Joshua Chen, Nadine Chang, Maying Shen, Zuxuan Wu, Shiyi Lan, and Jose M Alvarez. Generalized trajectory scoring for end-to-end multimodal planning. *arXiv preprint arXiv:2506.06664*, 2025f.

Zhiqi Li, Zhiding Yu, Shiyi Lan, Jiahan Li, Jan Kautz, Tong Lu, and Jose M Alvarez. Is ego status all you need for open-loop end-to-end autonomous driving? In *CVPR*, pp. 14864–14873, 2024c.

Bencheng Liao, Shaoyu Chen, Haoran Yin, Bo Jiang, Cheng Wang, Sixu Yan, Xinbang Zhang, Xiangyu Li, Ying Zhang, Qian Zhang, et al. Diffusiondrive: Truncated diffusion model for end-to-end autonomous driving. In *CVPR*, pp. 12037–12047, 2025.

Yiyi Liao, Jun Xie, and Andreas Geiger. Kitti-360: A novel dataset and benchmarks for urban scene understanding in 2d and 3d. *IEEE TPAMI*, 45(3):3292–3310, 2022.

Timothy P Lillicrap, Jonathan J Hunt, Alexander Pritzel, Nicolas Heess, Tom Erez, Yuval Tassa, David Silver, and Daan Wierstra. Continuous control with deep reinforcement learning. *arXiv preprint arXiv:1509.02971*, 2015.

Norman Mu, Jingwei Ji, Zhenpei Yang, Nate Harada, Haotian Tang, Kan Chen, Charles R Qi, Runzhou Ge, Kratarth Goel, Zoey Yang, et al. Most: Multi-modality scene tokenization for motion prediction. In *CVPR*, pp. 14988–14999, 2024.

Ghadi Nehme and Tejas Y Deo. Safe navigation: Training autonomous vehicles using deep reinforcement learning in carla. *arXiv preprint arXiv:2311.10735*, 2023.

Dennis Park, Rares Ambrus, Vitor Guizilini, Jie Li, and Adrien Gaidon. Is pseudo-lidar needed for monocular 3d object detection? In *Proceedings of the IEEE/CVF International Conference on Computer Vision*, pp. 3142–3152, 2021.

Tung Phan-Minh, Elena Corina Grigore, Freddy A Boulton, Oscar Beijbom, and Eric M Wolff. Covernet: Multimodal behavior prediction using trajectory sets. In *CVPR*, pp. 14074–14083, 2020.

Jonah Philion and Sanja Fidler. Lift, splat, shoot: Encoding images from arbitrary camera rigs by implicitly unprojecting to 3d. In *ECCV*, pp. 194–210. Springer, 2020.

Katrin Renz, Kashyap Chitta, Otniel-Bogdan Mercea, A. Sophia Koepke, Zeynep Akata, and Andreas Geiger. Plant: Explainable planning transformers via object-level representations. In *CoRL*, 2022.

John Schulman, Philipp Moritz, Sergey Levine, Michael Jordan, and Pieter Abbeel. High-dimensional continuous control using generalized advantage estimation. *arXiv preprint arXiv:1506.02438*, 2015.

Hao Shao, Letian Wang, Ruobing Chen, Hongsheng Li, and Yu Liu. Safety-enhanced autonomous driving using interpretable sensor fusion transformer. In *CoRL*, pp. 726–737. PMLR, 2023.

Zhihong Shao, Peiyi Wang, Qihao Zhu, Runxin Xu, Junxiao Song, Xiao Bi, Haowei Zhang, Mingchuan Zhang, YK Li, Yang Wu, et al. Deepseekmath: Pushing the limits of mathematical reasoning in open language models. *arXiv preprint arXiv:2402.03300*, 2024.

Chonghao Sima, Kashyap Chitta, Zhiding Yu, Shiyi Lan, Ping Luo, Andreas Geiger, Hongyang Li, and Jose M Alvarez. Centaur: Robust end-to-end autonomous driving with test-time training. *arXiv preprint arXiv:2503.11650*, 2025.

Pei Sun, Henrik Kretzschmar, Xerxes Dotiwalla, Aurelien Chouard, Vijaysai Patnaik, Paul Tsui, James Guo, Yin Zhou, Yuning Chai, Benjamin Caine, et al. Scalability in perception for autonomous driving: Waymo open dataset. In *CVPR*, pp. 2446–2454, 2020.

Richard S Sutton, Andrew G Barto, et al. *Reinforcement learning: An introduction*, volume 1. MIT press Cambridge, 1998.

Richard S Sutton, David McAllester, Satinder Singh, and Yishay Mansour. Policy gradient methods for reinforcement learning with function approximation. *NeurIPS*, 12, 1999.

Marin Toromanoff, Emilie Wirbel, and Fabien Moutarde. End-to-end model-free reinforcement learning for urban driving using implicit affordances. In *CVPR*, pp. 7153–7162, 2020.

Ashish Vaswani, Noam Shazeer, Niki Parmar, Jakob Uszkoreit, Llion Jones, Aidan N Gomez, Łukasz Kaiser, and Illia Polosukhin. Attention is all you need. *NeurIPS*, 30, 2017.

Junming Wang, Xingyu Zhang, Zebin Xing, Songen Gu, Xiaoyang Guo, Yang Hu, Ziying Song, Qian Zhang, Xiaoxiao Long, and Wei Yin. He-drive: Human-like end-to-end driving with vision language models. *arXiv preprint arXiv:2410.05051*, 2024.

Zi Wang, Shiyi Lan, Xinglong Sun, Nadine Chang, Zhenxin Li, Zhiding Yu, and Jose M Alvarez. Enhancing autonomous driving safety with collision scenario integration. *arXiv preprint arXiv:2503.03957*, 2025.

Penghao Wu, Xiaosong Jia, Li Chen, Junchi Yan, Hongyang Li, and Yu Qiao. Trajectory-guided control prediction for end-to-end autonomous driving: A simple yet strong baseline. *NeurIPS*, 35:6119–6132, 2022.

Pengchuan Xiao, Zhenlei Shao, Steven Hao, Zishuo Zhang, Xiaolin Chai, Judy Jiao, Zesong Li, Jian Wu, Kai Sun, Kun Jiang, et al. Pandaset: Advanced sensor suite dataset for autonomous driving. In *ITSC*, pp. 3095–3101. IEEE, 2021.

Lihe Yang, Bingyi Kang, Zilong Huang, Xiaogang Xu, Jiashi Feng, and Hengshuang Zhao. Depth anything: Unleashing the power of large-scale unlabeled data. *arXiv preprint arXiv:2401.10891*, 2024.

Zhenjie Yang, Xiaosong Jia, Qifeng Li, Xue Yang, Maoqing Yao, and Junchi Yan. Raw2drive: Reinforcement learning with aligned world models for end-to-end autonomous driving (in carla v2). *arXiv preprint arXiv:2505.16394*, 2025.

Wenhao Yao, Zhenxin Li, Shiyi Lan, Zi Wang, Xinglong Sun, Jose M Alvarez, and Zuxuan Wu. Drivesuprim: Towards precise trajectory selection for end-to-end planning. *arXiv preprint arXiv:2506.06659*, 2025.

Zhejun Zhang, Alexander Liniger, Dengxin Dai, Fisher Yu, and Luc Van Gool. End-to-end urban driving by imitating a reinforcement learning coach. In *ICCV*, pp. 15222–15232, 2021.

Hongyu Zhou, Longzhong Lin, Jiabao Wang, Yichong Lu, Dongfeng Bai, Bingbing Liu, Yue Wang, Andreas Geiger, and Yiyi Liao. Hugsim: A real-time, photo-realistic and closed-loop simulator for autonomous driving. *arXiv preprint arXiv:2412.01718*, 2024.